Multiconductor Transmission-Line Characterization: Representations, Approximations, and Accuracy

Dylan F. Williams, *Senior Member, IEEE*, Janet E. Rogers, and Christopher L. Holloway, *Member, IEEE*

***Abstract*—This paper investigates a measurement method that characterizes lossy printed multiconductor transmission lines, its accuracy, the choice of measurement representations, and some simple approximations. We illustrate the method with measurements of a pair of lossy coupled asymmetric microstrip lines.**

***Index Terms*—Measurement, modal cross power, multiconductor transmission line.**

I. Introduction

THIS PAPER investigates the measurement method of [1], which characterizes multiconductor transmission lines in the modal and "power-normalized" conductor representations of [2] and [3]. We present a comparison of the modal and power-normalized representations, discuss measurement accuracy, and investigate approximations suitable for use in digital simulators.

The measurement method is based on the electrical model of Fig. 1 for a multiconductor transmission line under test. This model embeds the lines in two reciprocal four-port "error boxes" to account for transition parasitics between the measurement reference planes, which are located in the access lines of Fig. 2, and the multiconductor transmission line itself. The measurement procedure uses two-port data and the weighted orthogonal distance regression algorithm of [4] to best determine the parameters of the error boxes and transmission line.

The procedure consists of three steps. The first step calibrates an overdetermined set of two-port measurement data in the access lines. The second finds the low-frequency limit $\boldsymbol{C}_{c0}$ of the line's matrix $\boldsymbol{C}_c$ of capacitances per unit length in its power-normalized representation. This step makes use of measurements of both sections of the multiconductor transmission line and of resistors embedded in it to estimate $\boldsymbol{C}_{c0}$. This estimate is based on the assumption that the resistors' power-normalized impedance matrices approach their dc impedance matrices at low frequencies.

The third step of the procedure is based on the fact that the matrix $\boldsymbol{Y}_c$ of transmission-line admittances per unit length in the conductor representation is easily approximated from $\boldsymbol{C}_{c0}$ over the entire frequency range. Fixing $\boldsymbol{Y}_c$ defines the impedance normalization of the conductor representation and allows all of the parameters of the electrical model to be determined uniquely from measurements of multiconductor transmission-line sections without recourse to the low-frequency approximations of the second step. This approach

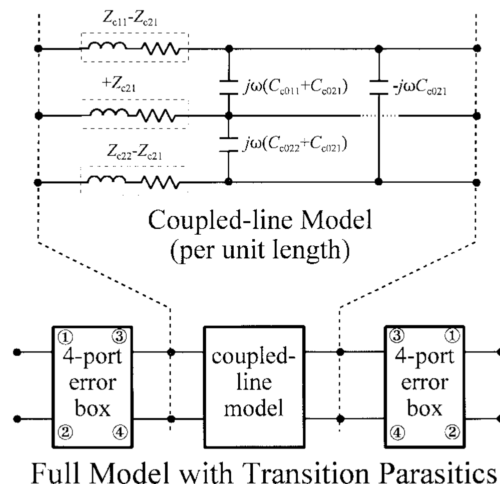

Fig. 1. Full model of the measured lines. The model includes a multiconductor transmission line and two four-port error boxes to account for transition parasitics. The two error boxes were electrically identical, except for their connections, which are indicated by the circled terminal numbers marked in the figure.

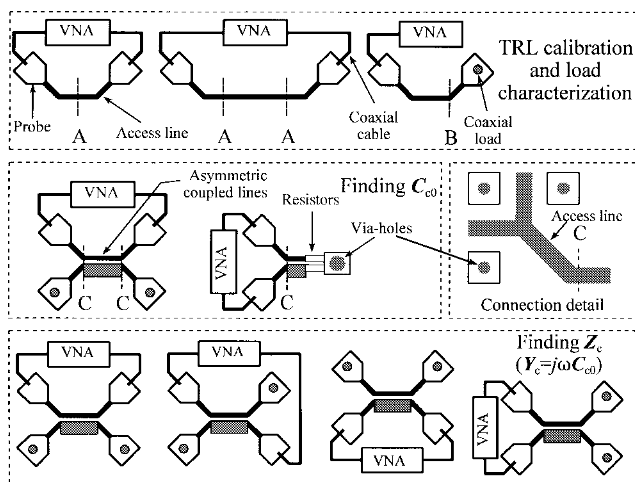

Fig. 2. Schematic representation of the measurement artifacts and procedure. Coaxial cables connect the vector network analyzer (VNA) to the probes. The probes contact the center conductor of the access lines directly. The inset labeled "Connection detail" shows the contacts, via holes, and Y junction used to contact the access lines.

Manuscript received December 5, 1997; revised January 26, 1999.

D. F. Williams and J. E. Rogers are with the National Institute of Standards and Technology, U.S. Department of Commerce, Boulder Laboratories, Boulder, CO 80303 USA.

C. L. Holloway is with the Institute for Telecommunications Sciences, U.S. Department of Commerce, Boulder Laboratories, Boulder, CO 80303 USA.

Publisher Item Identifier S 0018-9480(99)02994-4.

U.S. Government work not protected by U.S. copyright.

not only determines all of the parameters describing the transition parasitics modeled by the error boxes and the parameters describing the transmission line in both its modal and conductor representations, but also eliminates the requirement of the approach presented in [5] that the relationships between the modal and conductor voltages be fixed by symmetry and that these relationships be known in advance.

In this paper, we will describe the measurement method, study its accuracy, and investigate an expression for estimating parameters characterizing multiconductor transmission lines suitable for efficient digital simulation. We will also use measurements of a pair of lossy coupled asymmetric microstrip lines to illustrate the properties of the modal and power-normalized conductor representations.

II. Transmission-Line Modes

The total transverse electric field $\boldsymbol{E}_{\rm t}$ and magnetic field $\boldsymbol{H}_{\rm t}$ in a closed transmission line that is uniform in z and constructed of linear isotropic materials can be written as [6]

$$\boldsymbol{E}_{\rm t} = \sum_n \frac{v_{{\rm m}n}}{v_{0n}} \boldsymbol{e}_{{\rm t}n}$$
$$\boldsymbol{H}_{\rm t} = \sum_n \frac{i_{{\rm m}n}}{i_{0n}} \boldsymbol{h}_{{\rm t}n}. \tag{1}$$

Here, $v_{{\rm m}n}$ and $i_{{\rm m}n}$ are the modal voltages and currents and are functions only of z, v_{0n}, and i_{0n} normalize $v_{{\rm m}n}$ and $i_{{\rm m}n}$, and $\boldsymbol{e}_{{\rm t}n}$ and $\boldsymbol{h}_{{\rm t}n}$ are the transverse modal electric and magnetic fields and are functions only of the transverse coordinates x and y. The subscript $\rm m$ indicates that the quantities are modal and the sums over the modes n span all of the excited modes in the line. The time–harmonic dependence $e^{+j\omega t}$, where ω is the real angular frequency, has been suppressed. In open guides, we must add a continuous spectrum of modes to this discrete set [7], which we assume we can neglect here.

We restrict the normalizing voltages v_{0n} and currents i_{0n} by setting $v_{0n} i_{0n}^* = p_{0n} \equiv \int_S \boldsymbol{e}_{{\rm t}n} \times \boldsymbol{h}_{{\rm t}n}^* \cdot \boldsymbol{z}\, dS$, where $\mathrm{Re}(p_{0n}) \geq 0$, so that the power carried in the forward direction by the nth forward and backward modes in the absence of any other modes in the guide is given by $v_{{\rm m}n} i_{{\rm m}n}^*$; this is the conventional normalization and corresponds to the power condition used in [2] and [8] and suggested by Brews [9]. The characteristic impedance of the nth mode is $Z_{0n} \equiv v_{0n}/i_{0n} = |v_{0n}|^2/p_{0n}^* = p_{0n}/|i_{0n}|^2$; its magnitude is fixed by the choice of $|v_{0n}|$ or $|i_{0n}|$ while its phase is fixed by p_{0n}.

The vectors of modal voltages $\boldsymbol{v}_{\rm m}$ and modal currents $\boldsymbol{i}_{\rm m}$ satisfy the transmission-line equations

$$\frac{d\boldsymbol{v}_{\rm m}}{dz} = -\boldsymbol{Z}_{\rm m} \boldsymbol{i}_{\rm m}$$
$$\frac{d\boldsymbol{i}_{\rm m}}{dz} = -\boldsymbol{Y}_{\rm m} \boldsymbol{v}_{\rm m} \tag{2}$$

where the diagonal matrices of modal impedances and admittances per unit length are $\boldsymbol{Z}_{\rm m} \equiv \boldsymbol{\gamma} \boldsymbol{Z}_0$ and $\boldsymbol{Y}_{\rm m} \equiv \boldsymbol{\gamma} \boldsymbol{Z}_0^{-1}, \gamma = \mathrm{diag}(\gamma_n)$ is the diagonal matrix of modal propagation constants γ_n, and $\boldsymbol{Z}_0 = \mathrm{diag}(Z_{0n})$ [2].

When a finite number of the discrete modes are excited in the line, the total complex power p carried in the forward direction is

$$\begin{aligned} p &= \int \boldsymbol{E}_{\rm t} \times \boldsymbol{H}_{\rm t}^* \cdot \boldsymbol{z}\, dS \\ &= \sum_{n,k} \frac{v_{{\rm m}n}}{v_{0n}} \frac{i_{{\rm m}k}^*}{i_{0k}^*} \int \boldsymbol{e}_{{\rm t}n} \times \boldsymbol{h}_{{\rm t}k}^* \cdot \boldsymbol{z}\, dS \\ &= \boldsymbol{i}_{\rm m}^\dagger \boldsymbol{X} \boldsymbol{v}_{\rm m} \end{aligned} \tag{3}$$

where the superscript † indicates the Hermitian adjoint (conjugate transpose), the elements of the cross-power matrix $\boldsymbol{X}$ are defined by $X_{nk} \equiv (v_{0k} i_{0n}^*)^{-1} \int \boldsymbol{e}_{{\rm t}k} \times \boldsymbol{h}_{{\rm t}n}^* \cdot \boldsymbol{z}\, dS, X_{nn} = 1$, and the integrals are performed over the entire transmission-line cross section [2].

III. Conductor Representation

Since every mode excited in a multiconductor transmission line will impress a voltage across each of its conductors, the total voltage between any given conductor pair will be a linear combination of the modal voltages. Likewise, the total current in any given conductor will be a linear combination of the modal currents. References [2] and [3] refer to these linear combinations of modal voltages and currents as the "conductor" voltages and currents.

The vectors of conductor voltages $\boldsymbol{v}_{\rm c}$ and currents $\boldsymbol{i}_{\rm c}$ of [2] and [3] are defined by $\boldsymbol{v}_{\rm c} \equiv \boldsymbol{M}_{\rm v} \boldsymbol{v}_{\rm m}$ and $\boldsymbol{i}_{\rm c} \equiv \boldsymbol{M}_{\rm i} \boldsymbol{i}_{\rm m}$, where the subscript $\rm c$ indicates a conductor quantity, the matrices $\boldsymbol{M}_{\rm v}$ and $\boldsymbol{M}_{\rm i}$ are unitless, and, except in some special cases, are frequency dependent. The vectors $\boldsymbol{v}_{\rm c}$ and $\boldsymbol{i}_{\rm c}$ are power normalized in [2] and [3] so that $p = \boldsymbol{i}_{\rm c}^\dagger \boldsymbol{v}_{\rm c}$: this requires that $\boldsymbol{M}_{\rm v}$ and $\boldsymbol{M}_{\rm i}$ satisfy $\boldsymbol{M}_{\rm i}^\dagger \boldsymbol{M}_{\rm v} = \boldsymbol{X}$. The vectors $\boldsymbol{v}_{\rm c}$ and $\boldsymbol{i}_{\rm c}$ satisfy the transmission-line equations [2]

$$\frac{d\boldsymbol{v}_{\rm c}}{dz} = -\boldsymbol{Z}_{\rm c} \boldsymbol{i}_{\rm c}$$
$$\frac{d\boldsymbol{i}_{\rm c}}{dz} = -\boldsymbol{Y}_{\rm c} \boldsymbol{v}_{\rm c} \tag{4}$$

where the matrices of conductor impedances and admittances per unit length are defined by

$$\boldsymbol{Z}_{\rm c} \equiv \boldsymbol{R}_{\rm c} + j\omega \boldsymbol{L}_{\rm c} \equiv \boldsymbol{M}_{\rm v} \boldsymbol{Z}_{\rm m} \boldsymbol{M}_{\rm i}^{-1}$$

and

$$\boldsymbol{Y}_{\rm c} \equiv \boldsymbol{G}_{\rm c} + j\omega \boldsymbol{C}_{\rm c} \equiv \boldsymbol{M}_{\rm i} \boldsymbol{Y}_{\rm m} \boldsymbol{M}_{\rm v}^{-1}.$$

IV. Measurement Method

Fig. 2 illustrates the data acquisition and analysis procedure, which begin with a two-port multiline thru-reflect-line (TRL) calibration [10] with reference impedance correction [11] in microstrip access lines. We used on-wafer probes to connect to these access lines, employing conventional via holes through the substrate to form the electrical connection to the ground plane on the back of the substrate. To simplify the connections, we placed a "Y" junction in the access line and additional contacts and vias, as illustrated in the inset of Fig. 2, labeled "Connection detail." These additional contacts and vias allow

TABLE I
MEASURED AND CALCULATED ELEMENTS OF C_{c0} AND C_{c2}

i	j	Measured C_{c0ij} (pF/cm)	Calculated C_{c2ij} (pF/cm)/(GHz^2)	$\omega^2 C_{c2ij}/C_{c0ij}$ at 10 GHz
1	1	1.116	-1.13×10^{-6}	~0.004
2	2	1.986	-3.62×10^{-6}	~0.007
1	2	-0.514	0	0

the access lines to be contacted from either of two orthogonal directions by the probes.

This initial TRL calibration corrects for errors in the two-port data due to imperfections in the analyzer. The calibration also removes the effects of the wafer probes, via-hole transitions, Y junctions, and access lines used to connect the analyzer to the multiconductor lines; this eliminates the need for the models required in [5] to account for the contacts, via-hole transitions, and access lines. However this calibration does not take into account coupling between the access lines, the discontinuity where they connect to the multiconductor transmission line, or higher order mode excitation at that discontinuity: these effects will be accounted for by the four-port error boxes (see Fig. 1).

The initial reference plane of the TRL calibration is in the middle of the shortest line, marked A in the upper box of Fig. 2. Measurements at the reference plane marked B determine the impedances of a set of imperfect loads, each of which consisted of a section of the access line, Y junction, probe, and coaxial load.

During the collection of the two-port measurement data, the on-wafer probes contacted the access lines at two of the four transmission-line ports; the imperfect, but already characterized, loads are used to terminate the remaining access lines. This is illustrated in the middle and lower boxes of Fig. 2, which schematically show how the analyzer and loads were connected to the lines and resistors during the two optimization steps. In both optimizations, we use all four of the transmission-line measurement configurations, shown in the lower part of Fig. 2.

The first optimization of the procedure is illustrated in the middle box of Fig. 2. We estimate values of $\boldsymbol{Z}_{\rm c}$ and $\boldsymbol{Y}_{\rm c}$ using orthogonal distance regression [4]; the optimized values are those that minimize the sum of the squared differences between the model of Fig. 1 and the measured two-port impedance matrices of resistors and sections of the lines terminated with characterized loads. The reference plane for the two-port measurement data is at C, and the algorithm uses the assumption that the impedance matrices of the embedded resistors are equal to their measured dc impedance matrices. Then $\boldsymbol{C}_{\rm c0}$ is determined from a low-frequency extrapolation of $\boldsymbol{Y}_{\rm c}$: this works because the approximation for the impedance matrices of the embedded resistors is good at low frequencies.

The second optimization is illustrated in the lower box of Fig. 2. Here, we set $\boldsymbol{Y}_{\rm c}$ to $j\omega(\boldsymbol{C}_{\rm c0}+\omega^2\boldsymbol{C}_{\rm c2})$ and resolved for $\boldsymbol{Z}_{\rm c}$. We determined the elements of $\boldsymbol{C}_{\rm c2}$ listed in Table I with the full-wave method of [12]. These values are small compared to the elements of $\boldsymbol{C}_{\rm c0}$, and had little effect on the final measured results. Setting $\boldsymbol{Y}_{\rm c}$ in this way fixes the impedance normalization of the conductor representation.

Setting $\boldsymbol{Y}_{\rm c}$ also eliminates the requirement for the extra resistor measurements and associated approximations needed to solve uniquely for the parameters describing the error boxes in the first optimization [1]. These error boxes account for the coupling between the access lines, the discontinuity at the junction to the multiconductor transmission line, and for any higher order mode excitation at that junction. Explicitly incorporating them in the measurement model insures that these parasitic elements do not introduce systematic error into the transmission-line parameters.

To fit the two-port measurement data, we needed to determine the impedance matrix $\boldsymbol{Z}_{\rm ct}$ of sections of the multiconductor transmission line as a function of $\boldsymbol{Z}_{\rm c}$ and $\boldsymbol{Y}_{\rm c}$. To determine $\boldsymbol{Z}_{\rm ct}$, we used the fact that $\boldsymbol{M}_{\rm v}$ and $\boldsymbol{M}_{\rm i}$ diagonalize $\boldsymbol{Z}_{\rm c}\boldsymbol{Y}_{\rm c}\equiv\boldsymbol{M}_{\rm v}\boldsymbol{\gamma}^2\boldsymbol{M}_{\rm v}^{-1}$ and $\boldsymbol{Y}_{\rm c}\boldsymbol{Z}_{\rm c}\equiv\boldsymbol{M}_{\rm i}\boldsymbol{\gamma}^2\boldsymbol{M}_{\rm i}^{-1}$, which implies that the eigenvalues of $\boldsymbol{Z}_{\rm c}\boldsymbol{Y}_{\rm c}$ (or $\boldsymbol{Y}_{\rm c}\boldsymbol{Z}_{\rm c}$) determine $\boldsymbol{\gamma}$, the columns of $\boldsymbol{M}_{\rm v}$ are proportional to the eigenvectors of $\boldsymbol{Z}_{\rm c}\boldsymbol{Y}_{\rm c}$ and the columns of $\boldsymbol{M}_{\rm i}$ are proportional to the eigenvectors of $\boldsymbol{Y}_{\rm c}\boldsymbol{Z}_{\rm c}$ [2]. The lines we studied support two dominant modes, which are commonly called the c and π modes, and which correspond to the even and odd modes in the symmetric case. We determined the proportionality constants needed to fix the columns of $\boldsymbol{M}_{\rm v}$ from the conditions $M_{\rm v2c}=1$ and $M_{{\rm v}1\pi}+M_{{\rm v}2\pi}=-1$. These conditions define the c-mode voltage equal to that between the second microstrip conductor and the ground plane and the π-mode voltage equal to the difference of the voltages between the first and second microstrip conductors [13]. We determine the proportionality constants needed to fix the columns of $\boldsymbol{M}_{\rm i}$ from the relation $\boldsymbol{M}_{\rm i}^{\dagger}\boldsymbol{M}_{\rm v}=\boldsymbol{X}$, whose diagonal elements are all equal to one.

Once $\boldsymbol{\gamma}$, $\boldsymbol{M}_{\rm v}$, and $\boldsymbol{M}_{\rm i}$ were known, we determined the modal parameters describing the line from $\boldsymbol{Z}_{\rm m}\equiv\boldsymbol{M}_{\rm v}^{-1}\boldsymbol{Z}_{\rm c}\boldsymbol{M}_{\rm i}$, $\boldsymbol{Y}_{\rm m}\equiv\boldsymbol{M}_{\rm i}^{-1}\boldsymbol{Y}_{\rm c}\boldsymbol{M}_{\rm v}$, and $\boldsymbol{Z}_0\equiv\boldsymbol{\gamma}^{-1}\boldsymbol{Z}_{\rm m}$. We then determined the four-port impedance conductor matrix $\boldsymbol{Z}_{\rm ct}$ of the sections of the multimode transmission line from

$$\boldsymbol{Z}_{\rm ct}=\begin{bmatrix}\boldsymbol{M}_{\rm v}\boldsymbol{Z}_0\coth(\boldsymbol{\gamma}l)\boldsymbol{M}_{\rm i}^{-1} & \boldsymbol{M}_{\rm v}\boldsymbol{Z}_0\sinh(\boldsymbol{\gamma}l)^{-1}\boldsymbol{M}_{\rm i}^{-1}\\ \boldsymbol{M}_{\rm v}\boldsymbol{Z}_0\sinh(\boldsymbol{\gamma}l)^{-1}\boldsymbol{M}_{\rm i}^{-1} & \boldsymbol{M}_{\rm v}\boldsymbol{Z}_0\coth(\boldsymbol{\gamma}l)\boldsymbol{M}_{\rm i}^{-1}\end{bmatrix} \quad (5)$$

where l is its length, and the matrices $\coth(\boldsymbol{\gamma}l)\equiv\mathrm{diag}(\coth(\gamma_j l))$ and $\sinh(\boldsymbol{\gamma}l)^{-1}\equiv\mathrm{diag}(1/\sinh(\gamma_j l))$ are diagonal. From $\boldsymbol{Z}_{\rm ct}$, we calculated the two-port impedance matrices predicted by the model using Kirchhoff's laws and compared them to the two-port measurement data.

We also determined $\boldsymbol{X}$ from $\boldsymbol{X}=\boldsymbol{M}_{\rm i}^{\dagger}\boldsymbol{M}_{\rm v}$. Thus, although the method optimizes the conductor parameters $\boldsymbol{Z}_{\rm c}$ and $\boldsymbol{Y}_{\rm c}$ until the predictions of the model agree with the two-port measurement data, it determines the modal parameters at the same time and, thus, provides a complete description of the multiconductor transmission line in both representations.

V. Modal and Conductor Impedance Parameters

We applied the measurement procedure to two asymmetric coupled microstrip lines separated by a gap of 45 μm printed on a 254-μm-thick alumina substrate. The first microstrip

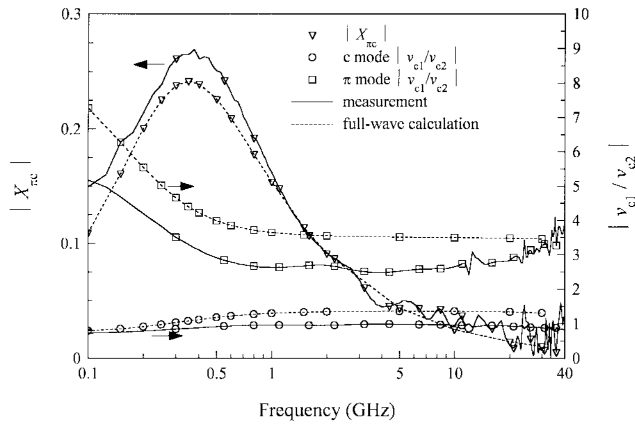

Fig. 3. Magnitude of $X_{\pi c}$ and ratios of the voltages impressed by the c and π modes between the 54-μm-wide microstrip conductor and the ground (v_{c1}) and the 254-μm-wide microstrip conductor and the ground (v_{c2}). The measurements were performed using the method of [1] and the calculations performed with the full-wave method of [12]. The arrows indicate the appropriate scales for the plotted data.

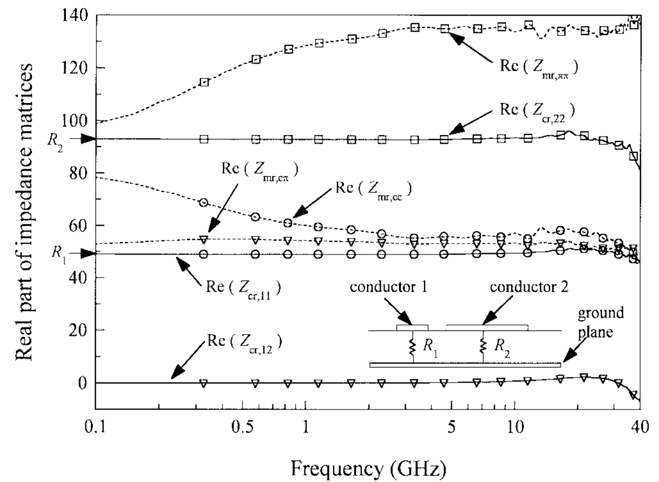

Fig. 4. Real part of the elements of the modal impedance matrix $Z_{\rm mr}$ and the conductor impedance matrix $Z_{\rm cr}$ for two small resistors. The connections of the resistors are sketched in the lower right of the figure; their measured dc resistances were $R_1 = 49\ \Omega$ and $R_2 = 93\ \Omega$ and are indicated with arrows on the left-hand side of the figure. (From [15].)

conductor had a width of 54 μm and the second a width of 254 μm. The lines had lengths of 1, 6, 11, 16, and 21 mm, and their conductor metallization had a measured thickness of 1.8 μm and measured dc conductivity of $3.3 \times 10^7\ \Omega^{-1} \cdot \mathrm{m}^{-1}$.

Fig. 3 compares measurements of the off-diagonal elements of $\boldsymbol{X}$ to full-wave calculations and shows fair agreement. It also shows that the ratios of the voltages impressed by the c and π modes between the two conductors and their grounds are frequency dependent. This is a reflection of the complex changes in the modal field configurations near the peak in the off-diagonal elements of $\boldsymbol{X}$ near 300 MHz. The physical phenomena responsible for this complex behavior are investigated by [14].

Fig. 3 not only illustrates the ability of the method to determine modal parameters, but also clearly shows two important drawbacks of the modal representation for circuit design: the modal field patterns are frequency dependent and, since $\boldsymbol{X}$ is not diagonal, the complex power is not equal to $\boldsymbol{i}_{\rm m}^{\dagger}\boldsymbol{v}_{\rm m}$.

We can illustrate these drawbacks in a more concrete way by examining the impedance matrices of the simple resistive circuit illustrated in the lower right corner of Fig. 4. The two small planar resistors were connected between the two conductors of the line and the ground plane on the back of the substrate with via-holes and had measured dc resistances of 49 and 93 Ω. We used the model of Fig. 1 and the procedure described in [15] to determine the circuit's modal and conductor impedance matrices.

The dashed lines in Fig. 4 correspond to the real parts of the measured elements of the modal impedance matrix $\boldsymbol{Z}_{\rm mr}$ of this small lumped circuit: they are highly frequency dependent. This illustrates another difficulty of using modal impedance matrices for circuit design: their elements do not correspond to those anticipated from simple physical models such as those of [16], despite the small size and lumped nature of the circuit. Circuit design in this modal representation is difficult because the modal impedance matrices depend not only on the circuit connected to the line, but also on the complex frequency-dependent modal behavior illustrated in Fig. 3.

The solid lines of Fig. 4 correspond to the real parts of the elements of the conductor impedance matrix $\boldsymbol{Z}_{\rm cr}$ of the circuit. The figure shows that the real parts of the elements of $\boldsymbol{Z}_{\rm cr}$ are nearly constant with frequency and correspond closely to the measured dc resistances of the two small resistors, as we would expect from simple physical considerations [16]; the imaginary parts of the elements of $\boldsymbol{Z}_{\rm cr}$ start at zero and increase linearly with frequency, and also correspond to behavior we would anticipate from physical considerations. Since $\boldsymbol{v}_{\rm c}$ and $\boldsymbol{i}_{\rm c}$ are power normalized, the conductor impedance matrices can be used directly in conventional circuit simulators to predict circuit response and power flow [2].

VI. Accuracy

We estimated $\boldsymbol{L}_{\rm c}$ and $\boldsymbol{R}_{\rm c}$ from two-port measurement data using ODRPACK [17], an implementation of the weighted orthogonal distance regression algorithm of [4]. Although this software makes finding least-squares estimates relatively straightforward, two important issues had to be addressed before we were able to estimate $\boldsymbol{L}_{\rm c}$ and $\boldsymbol{R}_{\rm c}$ and their errors. Firstly, there was a problem of numerical instability. Secondly, because of the way the data are measured, the number of degrees of freedom in the optimization results had to be determined.

Numerical instability can arise for a number of reasons: here it was due to both colinearity and very large values of the elements of the impedance matrix $\boldsymbol{Z}_{\rm e}$ describing the transitions between the single-mode microstrip access lines and the multiconductor transmission lines we were testing. Both the colinearity and large element values were due to the electrical characteristics of the transitions, which we had designed to minimize their electrical effects; as a result, the error boxes of Fig. 1 were nearly transparent to electrical signals and values of $\boldsymbol{Z}_{\rm e}$ corresponding to shunt electrical elements were large. In addition, small parasitics could be

added to either the left- or right-hand sides of the error box with nearly indistinguishable results.

We eliminated infinite elements of $\boldsymbol{Z}_{\mathrm{e}}$ by multiplying all of the two-port scattering-parameter measurement data by a constant factor of 0.5, which was equivalent to attenuating these measurements by 6 dB. This forces the error boxes to look like electrical 6-dB attenuators rather than thru connections. It also verified the ability of the algorithm and error boxes to compensate for large transition parasitics.

The numerical instability related to the indistinguishability of adding parasitics at either the left- or right-hand sides of the nearly perfect error boxes could be handled in any one of several ways, all of which produce nearly identical solutions for $\boldsymbol{L}_{\mathrm{c}}$ and $\boldsymbol{R}_{\mathrm{c}}$. For the results reported here, we forced $Z_{\mathrm{e}11} = Z_{\mathrm{e}33}$ and $Z_{\mathrm{e}22} = Z_{\mathrm{e}44}$ during the optimization. The estimates of the effects of the series parasitic elements in the signal paths are thus evenly distributed between the left- and right-hand sides of the error boxes.

We examined random and systematic errors separately. We used ODRPACK to characterize the random error from an analysis of the redundant two-port data it used to estimate model parameters. This analysis allows ODRPACK to determine confidence intervals for the results based on the assumption that the sources of the random error are normally and independently distributed [17]. However, Davidson and MacKinnon [18] show that nonlinear least-squares methods like those implemented in ODRPACK produce minimum variance and consistent asymptotically linear estimators even when the errors are not normally distributed.

We used the calibration comparison method [19] to approximate the number of degrees of freedom in the estimated variance of the random errors. The analysis indicated that those errors contained a large component due to drift in the electrical parameters describing the instrument, which led us to believe that they were highly correlated. Consistent with this analysis, we treated the data from each two-port measurement as having only two independent sources of random error. This assumption results in a reduction in the number of degrees of freedom and a slight increase in the estimated confidence intervals for the optimized parameters over what would be calculated if the data from each measured scattering parameter was considered to have an independent source of error.

Figs. 5 and 6 plot the measured values of $\boldsymbol{R}_{\mathrm{c}}$ and $\boldsymbol{L}_{\mathrm{c}}$ and their asymptotic 95% confidence intervals as determined by ODRPACK. The 95% intervals plotted in the figures reflect the confidence we have in these parameters under the assumption that the error sources in the experiment are entirely random.

We looked for systematic errors in our measurements of $\boldsymbol{R}_{\mathrm{c}}$ and $\boldsymbol{L}_{\mathrm{c}}$ by comparing their values to calculations performed with the full-wave method of [12], the most accurate numerical electromagnetic-field simulator of which we are aware. This simulator accounts not only for fringing fields and other high-frequency effects, but also for field penetration into the metals. These calculations are marked with crosses in Figs. 5 and 6.

A comparison of the full-wave calculations to the 95% intervals determined by ODRPACK detects the presence of additional systematic errors. Fig. 5 shows that the elements of the resistance matrix $\boldsymbol{R}_{\mathrm{c}}$ from the full-wave calculations

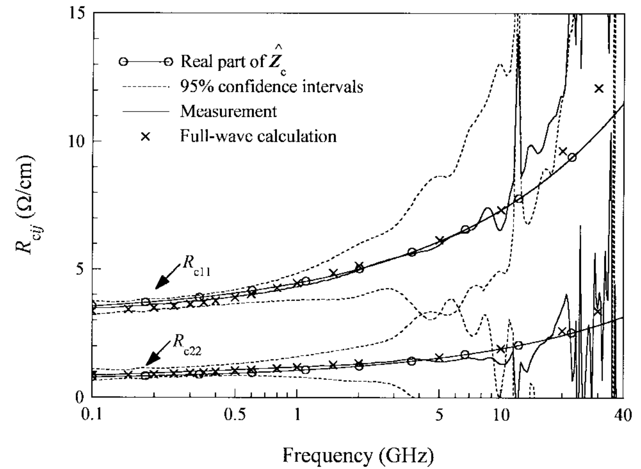

Fig. 5. Measured values of $\boldsymbol{R}_{\mathrm{c}}$ and their 95% confidence intervals compared to calculations from the full- wave method of [12] and the estimates $\hat{Z}_{\mathrm{c}}$.

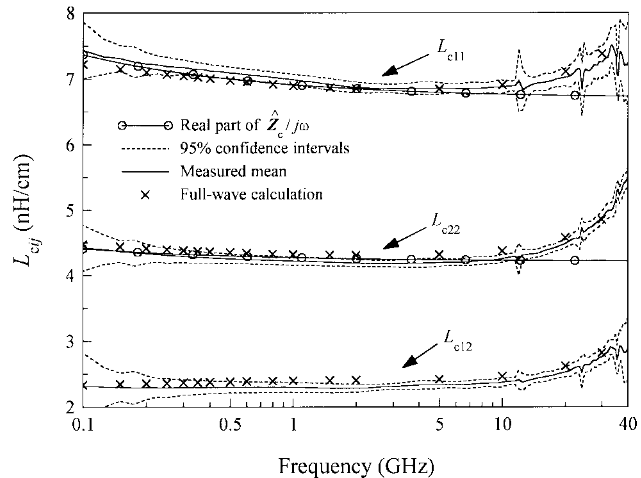

Fig. 6. Measured values of $\boldsymbol{L}_{\mathrm{c}}$ and their 95% confidence intervals compared to calculations from the full-wave method of [12] and the estimates $\hat{Z}_{\mathrm{c}}$.

fall well within the 95% confidence intervals over the entire frequency range. This indicates that the random error in these resistance measurements is far larger than any systematic errors in the experiment. This is not surprising given the large sizes of the estimated confidence intervals for the elements of $\boldsymbol{R}_{\mathrm{c}}$ at high frequency, where the real part of $\boldsymbol{Z}_{\mathrm{c}} \equiv \boldsymbol{R}_{\mathrm{c}} + j\omega\boldsymbol{L}_{\mathrm{c}}$ is small compared to its imaginary part.

However, Fig. 6 shows differences of up to 5% between the measured and calculated elements of the inductance matrix $\boldsymbol{L}_{\mathrm{c}}$. Since some of these calculated inductances fall outside of the 95% confidence intervals for the estimated parameters, we conclude that the discrepancies cannot be due entirely to random measurement error. This implies the existence of small, but statistically significant, systematic errors in either the measurements or the calculations.

We were unable to determine a source of the systematic error in the measurements of $\boldsymbol{L}_{\mathrm{c}}$. However, for the purposes of the full-wave calculations, we assumed that the alumina substrate had a dielectric constant of ten and was lossless. Furthermore, we used additional material and geometrical parameters in these calculations that we could not determine to better than

5%. These values are a possible source of error in the full-wave calculations, and may account for the systematic difference between the measurements and calculations.

VII. Digital Simulation

We will investigate an approximate form of the measured frequency-dependent values of $\boldsymbol{R}_c$ and $\boldsymbol{L}_c$ that can greatly reduce the computational burden of digital simulation tools. The assumptions employed in this section play no role in either the measurement procedure or analysis.

References [20] and [21] show that the computational burden associated with accounting for a frequency-dependent $\boldsymbol{Z}_c$ in finite-difference time-domain digital simulations can be greatly reduced when $\boldsymbol{Z}_c$c can be approximated as

$$\hat{\boldsymbol{Z}}_c \equiv \boldsymbol{A}_1 + \sqrt{j\omega}\boldsymbol{A}_2 + j\omega\boldsymbol{A}_3 \quad (6)$$

where the matrices $\boldsymbol{A}_1$, $\boldsymbol{A}_2$, and $\boldsymbol{A}_3$ are real and frequency independent. $\hat{\boldsymbol{Z}}_c$ is well suited for use in these tools because it has a closed-form Laplace transform whose convolutions can be calculated efficiently [20] with Prony's method [22]. $\hat{\boldsymbol{Z}}_c$ is also causal, which makes it suitable for use in methods such as [23], which are based on Green s functions.

If $\hat{\boldsymbol{Z}}_c$ is to correspond to $\boldsymbol{Z}_c$ at its dc limit, then the matrix $\boldsymbol{A}_1$ must be set to $\boldsymbol{R}_{dc}$, the line's dc resistance matrix; if $\hat{\boldsymbol{Z}}_c$ is to correspond to $\boldsymbol{Z}_c$ at its high-frequency limit, then $\boldsymbol{A}_3$ must be set to $\boldsymbol{L}_e$, the line's matrix of external inductances. Equation (6) can now be expressed as

$$\hat{\boldsymbol{Z}}_c = \boldsymbol{R}_{dc}(1 + (1+j)\sqrt{\omega}\boldsymbol{F}) + j\omega\boldsymbol{L}_c \quad (7)$$

where $\boldsymbol{R}_{dc}$ can be measured directly and $\boldsymbol{L}_e$ can be determined from quasi-static methods that ignore losses and penetration of fields into the metals [24].

Figs. 5 and 6 show $\hat{\boldsymbol{Z}}_c$ calculated by setting the real part of the diagonal elements of (7) equal to the real part of the diagonal elements of $\boldsymbol{Z}_c$ calculated with the full-wave method of [12] at 10 GHz; i.e., we matched the two conductor resistances predicted (7) to their calculated values at 10 GHz. The figures show that this $\hat{\boldsymbol{Z}}_c$ approximates the measured and numerically calculated values of $\boldsymbol{R}_c$ and $\boldsymbol{L}_c$ well enough to be useful in many digital simulations, even though it somewhat underestimates the elements of $\boldsymbol{L}_c$ at high frequencies.

VIII. Conclusion

We presented a method for the measurement and characterization of lossy asymmetric printed multiconductor transmission lines, which are important components in electronic packages and interconnections. The method is based on rigorous relations between the transmission line's conductor representation, its modal representation, and its impedance matrix; this allows it to be used to characterize lossy asymmetric coupled lines in which the modal cross powers are significant and the relationships between the modal and conductor voltages and currents are complex and frequency dependent.

We used the measurement method to convincingly demonstrate the advantages of the power-normalized representation of [2] and [3] over modal representations. However, the power-normalized representation investigated here and the reciprocity-based representation of [25] are nearly identical in these asymmetric microstrip lines [2]; thus, our results indicate that either one of these representations could be used for circuit design in these lines.

We also studied measurement accuracy and examined the asymptotic confidence intervals of the estimated parameters. The optimization procedure solved for all of the parameters of the model of Fig. 1 at each frequency: no information about the behavior of the model at adjacent frequencies was considered. This is the typical approach for network analyzer calibration, where the electrical parameters of the error boxes describing the analyzer vary rapidly and unpredictably with frequency.

However, the error boxes we use describe only the coupling between the access lines and the electrical behavior of the small lumped transitions between the access lines and the coupled line: the initial TRL calibrations remove the effects of the analyzer, cables, probes, contacts, and access lines. As a result, the electrical parameters describing these error boxes vary smoothly with frequency. It should be possible to take advantage of the lumped behavior of these error boxes to improve the estimated values of $\boldsymbol{L}_c$ and $\boldsymbol{R}_c$.

We also illustrated how to develop expressions for estimating conductor resistances and inductances that may be useful in digital simulations. These expressions are useful because their parameters can be determined from a full-wave calculation at a single frequency.

Acknowledgment

The authors appreciate the contributions of S. Sercu and L. Martens, University of Ghent, Ghent, Belgium, who made possible the measurements reported in this paper.

References

[1] D. F. Williams, "Characterization of embedded multiconductor transmission lines," in *IEEE/MTT-S Int. Microwave Symp. Dig.*, June 10–12, 1997.

[2] D. F. Williams, L. A. Hayden, and R. B. Marks, "A complete multimode equivalent-circuit theory for electrical design," *J. Res. Natl. Bur. Stand.*, May 1997.

[3] N. Faché and D. De Zutter, "New high-frequency circuit model for coupled lossless and lossy waveguide structures," *IEEE Trans. Microwave Theory Tech.*, vol. 38, pp. 252–259, Mar. 1990.

[4] P. T. Boggs, R. H. Byrd, and R. D. Schnabel, "A stable and efficient algorithm for nonlinear orthogonal distance regression," *SIAM J. Sci. Stat. Comput.*, pp. 1052–1078, Nov. 1987.

[5] T. Winkel, L. S. Dutta, H. Grabinski, and E. Grotelueschen, "Determination of the propagation constant of coupled lines on chips based on high frequency measurements," in *IEEE Multi-Chip Module Conf. Dig.*, Santa Cruz, CA, Feb. 6–7, 1996, pp. 99–104.

[6] R. E. Collin, *Field Theory of Guided Waves*. New York: McGraw-Hill, 1960.

[7] G. Goubau, "On the excitation of surface waves," *Proc. IRE*, vol. 40, pp. 865–868, July 1952.

[8] R. B. Marks and D. F. Williams, "A general waveguide circuit theory," *J. Res. Natl. Bur. Stand.*, pp. 533–561, Sept./Oct. 1992.

[9] J. R. Brews, "Transmission line models for lossy waveguide interconnections in VLSI," *IEEE Trans. Electron Devices*, vol. ED-33, pp. 1356–1365, Sept. 1986.

[10] R. B. Marks, "A multiline method of network analyzer calibration," *IEEE Trans. Microwave Theory Tech.*, vol. 39, pp. 1205–1215, July 1991.

[11] R. B. Marks and D. F. Williams, "Characteristic impedance determination using propagation constant measurement," *IEEE Microwave Guided Wave Lett.*, vol. 1, pp. 141–143, June 1991.

[12] W. Heinrich, "Full-wave analysis of conductor losses on MMIC transmission lines," *IEEE Trans. Microwave Theory Tech.*, vol. 38, pp. 1468–1472, Oct. 1990.
[13] D. F. Williams, "Multiconductor transmission line characterization," *IEEE Trans. Comput., Packag., Manufact. Technol.*, vol. 20, pp. 129–132, May 1997.
[14] D. F. Williams and F. Olyslger, "Modal cross power in quasi-TEM transmission lines," *IEEE Microwave Guided Wave Lett.*, vol. 6, pp. 413–415, Nov. 1996.
[15] D. F. Williams, "Calibration in multiconductor transmission lines," in *48th ARFTG Conf. Dig.*, Orlando, FL, Dec. 4–6, 1996.
[16] D. K. Walker, D. F. Williams, and J. M. Morgan, "Planar resistors for probe station calibration," in *40th ARFTG Conf. Dig.*, Orlando, FL, Dec. 1991, pp. 68–81.
[17] P. T. Boggs, R. H. Byrd, J. E. Rogers, and R. B. Schnabel, "User's reference guide for ODRPACK Version 2.01: Software for weighted orthogonal distance regression," Nat. Inst. Stand., Boulder, CO, Nat. Inst. Stand. Technol. Internal Rep. 92-4834, 1992.
[18] R. Davidson and J. G. MacKinnon, *Estimation and Inference in Econometrics*. Oxford, U.K.: Oxford Univ. Press, 1993.
[19] D. F. Williams, R. B. Marks, and A. Davidson, "Comparison of on-wafer calibrations," in *38th ARFTG Conf. Dig.*, San Diego, CA, Dec. 1991.
[20] C. R. Paul, *Analysis of Multiconductor Transmission Lines*. New York: Wiley, 1994.
[21] K. S. Kunz and R. J. Luebbers, *The Finite Difference Time Domain Method in Electromagnetics*. Boca, FL: CRC Press, 1993.
[22] F. B. Hildebrand, *Introduction to Numerical Analysis*. New York: Dover, 1974, pp. 457–462.
[23] A. R. Djordjević, T. K. Sarkar, and R. F. Harrington, "Analysis of lossy transmission lines with arbitrary nonlinear terminal networks," *IEEE Trans. Microwave Theory Tech.*, vol. MTT-34, pp. 660–666, June 1986.
[24] R. F. Harrington and C. Wei, "Losses on multiconductor transmission lines in multilayered dielectric media," *IEEE Trans. Microwave Theory Tech.*, vol. MTT-32, pp. 705–710, July 1984.
[25] F. Olyslager, D. De Zutter, and A. T. de Hoop, "New reciprocal circuit model for lossy waveguide structures based on the orthogonality of the eigenmodes," *IEEE Trans. Microwave Theory Tech.*, vol. 42, pp. 2261–2269, Dec. 1994.

Dylan F. Williams (S'82–M'86–SM'90) received the Ph.D. degree in electrical engineering from the University of California at Berkeley, in 1986.

In 1989, he joined the Electromagnetic Fields Division, National Institute of Standards and Technology (NIST), Boulder, CO, where he currently develops metrology for the characterization of monolithic microwave integrated circuits and electronic interconnects. He has published over 60 technical papers.

Dr. Williams has received the Department of Commerce Bronze and Silver Medals, the Electrical Engineering Laboratory's Outstanding Paper Award, two ARFTG Best Paper Awards, the ARFTG Automated Measurements Technology Award, and the IEEE Morris E. Leeds Award.

Janet E. Rogers received the M.S. degree in computer science and the M.A. degree in economics from Colorado University, Boulder, in 1985 and 1988, respectively.

Since 1973, she has been a member of the NIST Information Technology Laboratory (and its predecessors), National Institute of Standards and Technology (NIST), Boulder, CO, since 1973. She is currently a member of the Optimization Group, Mathematical and Computational Sciences Division, NIST. She has co-authored both ODRPACK and STARPAC software packages. Her interests include nonlinear least squares and optimization, orthogonal distance regression, measures of nonlinearity, and statistical computing.

Christopher L. Holloway (S'86–M'92) was born in Chattanooga, TN, on March 26, 1962. He received the B.S. degree from the University of Tennessee, Chattanooga, in 1986, and the M.S. and Ph.D. degrees from the University of Colorado, Boulder, in 1988 and 1992, respectively, both in electrical engineering.

During 1992, he was a Research Scientist with Electro Magnetic Applications, Inc., Lakewood, CO, where his responsibilities included theoretical analysis and finite-difference time-domain modeling of various electromagnetic problems. From 1992 to 1994, he was with the National Center for Atmospheric Research (NCAR), Boulder, CO. While at NCAR, his duties included wave-propagation modeling, signal-processing studies, and radar systems design. Since 1994, he has been with the Institute for Telecommunication Sciences (ITS), U.S. Department of Commerce, Boulder, CO, where he is involved in wave-propagation studies. He is also on the Graduate Faculty at the University of Colorado, Boulder. His research interests include electromagnetic-field theory, wave propagation, guided-wave structures, remote sensing, numerical methods, and electromagnetic compatibility/electromagnetic interference (EMC/EMI) issues.

Dr. Holloway is a member of Commission A of the International Union of Radio Science. He is an Associate Editor on propagation for the IEEE TRANSACTIONS ON ELECTROMAGNETIC COMPATIBILITY.